

Liquid-Phase Hydrogenation of Citral over Pt/SiO₂ Catalysts

I. Temperature Effects on Activity and Selectivity

Utpal K. Singh and M. Albert Vannice¹

Department of Chemical Engineering, Pennsylvania State University, 107 Fenske Laboratory, University Park, Pennsylvania 16802-4400

Received September 3, 1999; revised December 16, 1999; accepted December 22, 1999

Liquid-phase hydrogenation of citral (3,7-dimethyl-2,6-octadienal) over Pt/SiO₂ catalysts was studied in the temperature and pressure ranges 298–423 K and 7–21 atm, respectively. The reaction kinetics were shown to be free of artifacts arising from transport limitations and poisoning effects. The reaction rate in hexane as the solvent exhibited an activity minimum at 373 K. The initial turnover frequency for citral disappearance over 1.44% Pt/SiO₂ catalyst at 20 atm H₂ pressure decreased from 0.19 s⁻¹ at 298 K to 0.02 s⁻¹ at 373 K, but exhibited normal Arrhenius behavior between 373 and 423 K with an activation energy of 7 kcal/mol. Reaction at 298 K produced substantial deactivation, with the rate decreasing by more than an order of magnitude during the first 4 h of reaction; however, reaction at temperatures greater than 373 K exhibited negligible deactivation and a constant rate up to citral conversions greater than 70%. These unusual temperature effects were modeled using Langmuir–Hinshelwood kinetics invoking dissociative adsorption of hydrogen, competitive adsorption between hydrogen and the organic compounds, and addition of the second hydrogen atom to each reactant as the rate-determining step. Decomposition of the unsaturated alcohol (either geraniol or nerol) was proposed to occur concurrently with the hydrogenation steps to yield adsorbed CO and carbonaceous species which cause the deactivation, but at higher temperatures these species could be removed from the Pt surface by desorption or rapid hydrogenation, respectively. The activity minimum observed in the present study is attributed to the relative rates of the alcohol decomposition reaction and CO desorption, with the decomposition reaction having an activation barrier lower than that for CO desorption. © 2000 Academic Press

INTRODUCTION

Approximately 50–100 kg of by-product can be produced for a single kilogram of product in the pharmaceutical and fine chemicals industry, with much of the by-product being present as inorganic salts arising from multistep syntheses using stoichiometric reductants or homogeneous catalysts (1). Selective hydrogenation of α,β -unsaturated aldehydes represents a broad class of industrially relevant reactions in

the specialty and fine chemicals industry where NaBH₄ is used as a stoichiometric reductant (2). Significant focus has been placed on studying selectivity in hydrogenation reactions of α,β -unsaturated aldehydes, and several reviews of this work have recently been published (3–5). Numerous vapor-phase hydrogenation studies conducted under differential conditions to obtain reaction kinetics have proved valuable in obtaining mechanistic information (6–14); however, liquid-phase hydrogenation studies reported in the literature have focused primarily on obtaining a qualitative understanding of the reaction by monitoring the effect of mono- and bimetallic catalysts on product distribution (15–17). There is scant literature that examines the influence of reaction parameters such as temperature, pressure, and transport limitations on kinetics of liquid-phase hydrogenation reactions, and this deficiency was voiced in a recent review by Gallezot and Richard on hydrogenation of α,β -unsaturated aldehydes (3).

The work of Lercher and co-workers represents one of the few attempts at examining the effect of various reaction parameters such as temperature, pressure, catalyst weight, and water concentration on the liquid-phase hydrogenation of α,β -unsaturated aldehydes (18, 19). Regardless, a number of questions still remain to be resolved including the significance of internal diffusion resistance, catalyst poisoning, and the role of intermediates during hydrogenation reactions. One important consideration is that many of the liquid-phase hydrogenation studies reported in the literature have been performed after an *ex situ* reduction of the catalyst, and proper precautions were not taken to remove dissolved oxygen from the liquid phase prior to the start of reaction. This can introduce various changes in the state of the catalyst and can also influence the reaction kinetics (20).

We have studied liquid-phase hydrogenation of citral (3,7-dimethyl-2,6-octadienal) over supported Pt catalysts. Citral has three unsaturated bonds including a conjugated C=C–C=O bond system and an isolated C=C bond. The reaction chemistry of citral hydrogenation is shown in Fig. 1, which also includes minor side products not routinely

¹ To whom correspondence should be addressed.

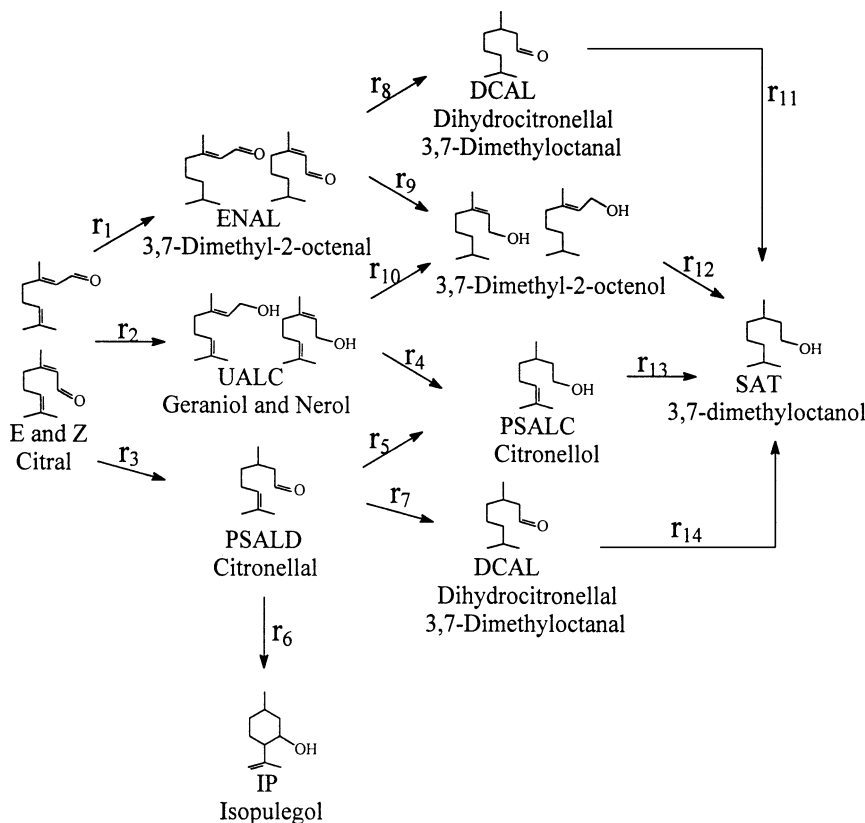


FIG. 1. Reaction chemistry for citral hydrogenation.

presented in the reaction pathways from previous reports (5). The two isomers of citral can undergo hydrogenation of the conjugated C=O functionality to yield the *cis* and *trans* isomers of the unsaturated alcohol (UALC), nerol and geraniol, respectively. Alternatively, both citral isomers can react via the conjugated C=C bond or the isolated C=C bond to yield either the partially saturated aldehyde (PSALD) or the *cis* and *trans* isomers of 3,7-dimethyl-2-octenal (ENAL), respectively. The latter product has not been confirmed unequivocally, but its presence has been inferred from mass spectral data and reaction kinetics as discussed in the subsequent paper (21). UALC and PSALD can undergo further hydrogenation of the remaining unsaturated bond in the initially conjugated system to yield the partially saturated alcohol (PSALC), which can subsequently be hydrogenated to yield the completely saturated product, 3,7-dimethyloctanol (SAT). PSALD can also react first via the isolated C=C species to yield dihydrocitronellal (DCAL) or it can isomerize with ring closure to yield isopulegol (IP). ENAL can undergo hydrogenation of either the C=O bond or the C=C bond to yield 3,7-dimethyl-2-octenol or DCAL, respectively. These two intermediates can further hydrogenate to yield the completely saturated product (SAT). In addition to the above reaction chemistry, some surface side reactions can also occur, as will be described later in this paper.

In the present investigation, a thorough, methodical study of liquid-phase hydrogenation of citral has been performed with the aim of obtaining quantitative kinetic data free of artifacts from transport resistance and catalyst poisoning. Particular emphasis has been placed on understanding the unusual effect of temperature on reaction rates and product distribution.

EXPERIMENTAL

SiO₂ (Davison grade 57, 220 m²/g, 60–100 mesh) was dried and calcined at 773 K for 4 h prior to impregnation. Three catalysts were prepared with hydrogen hexachloroplatinate(IV) hydrate (H₂PtCl₆, Aldrich 99.995%) as a precursor using the incipient wetness (IW) technique; i.e., an aqueous solution of chloroplatinic acid was added dropwise to a calcined support (2 cm³/g SiO₂) and subsequently dried at 393 K overnight. A 3.8% Pt/SiO₂ catalyst was prepared with Pt(NH₃)₄Cl₂ using an ion-exchange method. Hydrogen chemisorption was measured at 300 K in a static volumetric apparatus with a base pressure of 10⁻⁷ Torr using a procedure described elsewhere (22). All catalysts were reduced at 673 K for 75 min under flowing H₂. Although dual isotherms were obtained, Pt dispersions were calculated using the value of the total H₂ uptake isotherm extrapolated

TABLE 1
H₂ Chemisorption on Pt/SiO₂ Catalysts at 300 K

Catalyst	H ₂ uptake ($\mu\text{mol/gcat}$)		H _{Total} /Pt	<i>d</i> (nm)	Activity ($\mu\text{mol/g cat/min}$) ^a	Initial TOF (s ⁻¹) ^a
	(H ₂) _{Total}	(H ₂) _{Rev}				
2.65% Pt/SiO ₂	15.0	6.1	0.22	5.1	164	0.09
1.44% Pt/SiO ₂	15.2	7.4	0.41	2.8	27	0.017
0.49% Pt/SiO ₂	5.6	3.4	0.45	2.5	8	0.012
3.80% Pt/SiO ₂	64.1	24.6	0.66	1.7	53	0.007

^aReaction conditions: 373 K, 20 atm H₂, 1 M citral in hexane.

to zero pressure and assuming an adsorption stoichiometry of unity, i.e., a H_{ad}:Pt_s ratio of 1.

Hydrogenation experiments were conducted in a 100-ml EZ-seal autoclave with an automated data acquisition system that can monitor H₂ uptakes. Details have been provided elsewhere (23). The reactor was loaded with 0.5 to 1.0 g of catalyst, sealed, and leak tested at 54 atm to ensure a tight seal. Helium (MG Industries, 99.999%) was used as received while H₂ (MG Industries, 99.999%) was further purified by passage through a high-pressure Oxytrap (Alltech). Five pressure/vent cycles were conducted at room temperature by pressurizing the reactor to 54 atm in He followed by venting to atmospheric pressure to remove all traces of oxygen from inside the reactor. The pretreatment procedure was then initiated by flowing 200 cm³(STP)/min He over the catalyst while heating the reactor from room temperature to 673 K in 3 h. The flow was then switched to 500 cm³(STP)/min hydrogen for 75 min prior to cooling to room temperature and storing overnight under a static atmosphere of 20 psia H₂. This storage procedure had no effect on catalytic behavior as evidenced by identical turnover frequencies (TOFs) and product distributions, within experimental uncertainty, whether the catalyst was stored overnight or used immediately after the reduction.

The standard reaction conditions were 20 atm hydrogen pressure using 1 mol citral/liter in hexane with a total reaction volume of 60 ml. Citral (Sigma, 97%) and hexane were degassed by sparging with high flow rates of nitrogen for 30 min prior to injection into the reactor. Hexane (Fisher 99.9% saturated C₆ hydrocarbons) was fed into the reactor at reaction temperature and pressure using a high-pressure syringe pump (ISCO 500D) in a closed system to prevent any exposure to air. The hexane/catalyst slurry was stirred at 1000 rpm and allowed to equilibrate for 30 min prior to the introduction of citral to obtain a total reaction volume of 60 ml. The pressure was continuously maintained to within 5% of the set point with a Brooks 5860 pressure controller during these semi-batch reactor experiments, and the pressure decay within the 5% range, i.e., 315–300 psia, was monitored to obtain the instantaneous rate of H₂ uptake at any time during the reaction. In addition, a 0.5-ml liquid sample was periodically withdrawn through a dip tube

extending inside the reactor and collected in a closed, N₂-purged vessel, and it was then analyzed in a HP 5890 gas chromatograph equipped with a thermal conductivity detector and a 10% Carbowax 20M on Supelcoport packed column. Initial rates of citral disappearance were evaluated using the slope of the linear portion of the temporal citral conversion profile (for citral conversions less than 20%). The product selectivity was calculated as follows:

$$S_i = \frac{\text{concentration of species } i}{\sum_{\text{products}} \text{concentration of species } i} \quad [1]$$

RESULTS

Table 1 gives information about the catalysts and displays the H₂ chemisorption results and pretreatment procedures for the catalysts used. Two catalysts with similar dispersions (H/Pt ~ 0.4) but a threefold variation in platinum loading (0.49 and 1.44% Pt/SiO₂) were used to apply the Madon–Boudart test to check for the absence of heat and mass transport effects (24). The results of the test under standard conditions and 373 or 393 K are shown in Table 2. The equal TOFs, within experimental uncertainty, for citral disappearance on the two catalysts at two different reaction temperatures verify the absence of internal and external heat and mass transfer limitations. In addition, no catalyst deactivation was observed at these temperatures as evidenced by a constant hydrogenation rate as citral conversion varied from 10% to greater than 80%. Similar runs

TABLE 2

Madon–Boudart Test with 0.49% Pt/SiO₂ (H/Pt = 0.45) and 1.44% Pt/SiO₂ (H/Pt = 0.41) at 373 and 393 K, 20 atm H₂, and 1 M Citral in Hexane

	TOF (s ⁻¹)	
	373 K	393 K
0.49% Pt/SiO ₂	0.012	0.047
1.44% Pt/SiO ₂	0.017	0.049

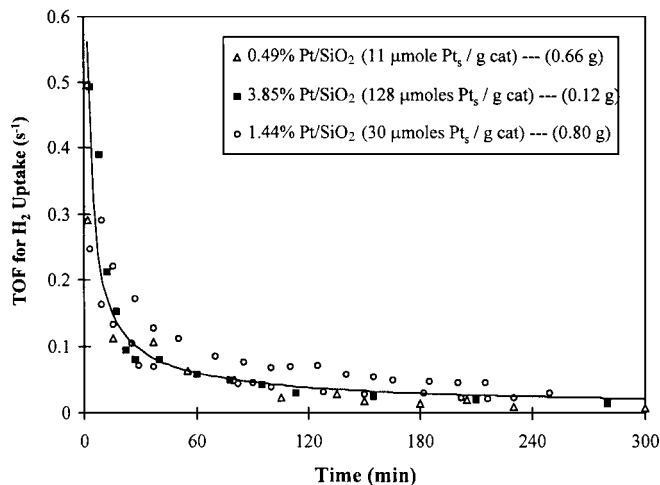


FIG. 2. Temporal H_2 uptake profiles during hydrogenation of 1 M citral in hexane at 298 K and 20 atm H_2 , over 0.49% Pt/SiO₂ (H/Pt = 0.45), 1.44% Pt/SiO₂ (H/Pt = 0.41), and 3.8% Pt/SiO₂ (H/Pt = 0.67) catalysts.

were conducted at 298 K and standard conditions with a series of catalysts whose concentration of surface Pt atoms varied by more than an order of magnitude from 11 μmol Pt₃/g cat for 0.49% Pt/SiO₂ to 128 μmol Pt₃/g cat for 3.8% Pt/SiO₂, and these results are presented in Fig. 2. The similar trend in TOF for H_2 uptake versus time for the three catalysts is additional evidence indicating the absence of artifacts due to transport limitations or poisoning effects at 298 K and 20 atm H_2 ; the obvious deactivation that is observed is attributed to a side reaction, as discussed later. Figures 3a and 3b show the effect of catalyst weight on the reaction kinetics during hydrogenation under standard conditions at 298 K using 1.44% Pt/SiO₂. Despite the eightfold difference in catalyst mass inside the reactor, the temporal H_2 uptake curves on a TOF basis are identical; however, substantial differences between the two runs are seen in Fig. 3b when the H_2 uptake is plotted versus citral conversion. Due to the strong deactivation/inhibition behavior, the reaction with 0.09 g catalyst yielded 6.5% citral conversion after 3 h of reaction as compared with 57% for the run with 0.81 g catalyst. The identical values during the initial stages of the reaction for the two runs reinforce the fact that there is no transport limitation related to the transfer of H_2 from the gas to the liquid phase (25).

Figure 4 illustrates the effect that the pretreatment procedure, regarding exposure to O₂, can have on the temporal conversion profile for the reaction under standard conditions at 373 K. The *in situ* pretreatment procedure was described under Experimental. Briefly, the 1.44% Pt/SiO₂ catalyst was reduced *in situ* at 673 K in flowing hydrogen, then cooled to reaction temperature in hydrogen. Degassed hexane was added to the reactor (ensuring the exclusion of oxygen) and the slurry was allowed to equilibrate for 30 min prior to adding degassed citral to commence the reaction. The *ex situ* pretreatment consisted of reducing

the catalyst at 673 K in flowing hydrogen and passivating it at 300 K with 5% O₂ in He using 100 cm³ (STP)/min before its subsequent exposure to air. The catalyst was transferred into the autoclave and purged first with helium and finally with hydrogen. The reactor temperature and pressure were then raised to 373 K and 20 atm H_2 at which time 50 cm³ hexane (with no degassing) was added. The hexane/catalyst slurry was stirred and allowed to equilibrate under H_2 for 60 min at the reaction temperature and pressure prior to the addition of citral (with no degassing) to commence the reaction. The initial rate of disappearance of citral on the *ex situ*-reduced catalyst (TOF = 0.007 s⁻¹) was one-third that on the *in situ*-reduced catalyst (TOF = 0.020 s⁻¹), which suggests either that the catalyst may not be completely activated following an *ex situ* reduction procedure or that low concentrations of water can affect the kinetics. In addition, a nonzero intercept was observed after either pretreatment method at 373 K. All results reported in the present study were obtained following *in situ* reduction of the catalyst at 673 K in hydrogen and degassing of citral and hexane with nitrogen prior to their introduction into the reactor.

Experiments were conducted to obtain the reaction orders in citral concentration and H_2 pressure for the initial

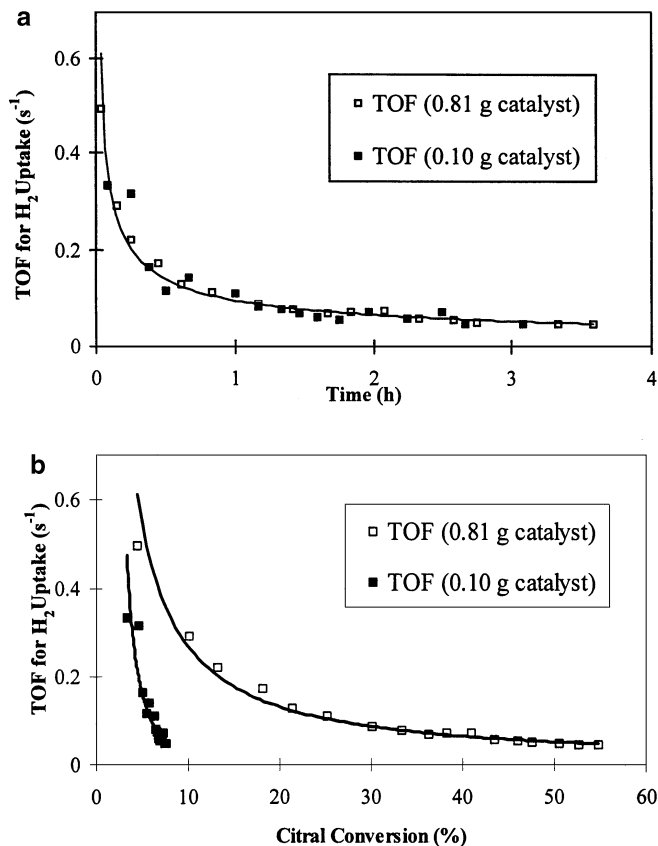


FIG. 3. Effect of catalyst weight on TOF for H_2 uptake during reaction at 298 K and 20 atm H_2 over 1.44% Pt/SiO₂ with 1 M citral in hexane (a) as a function of time and (b) as a function of citral conversion.

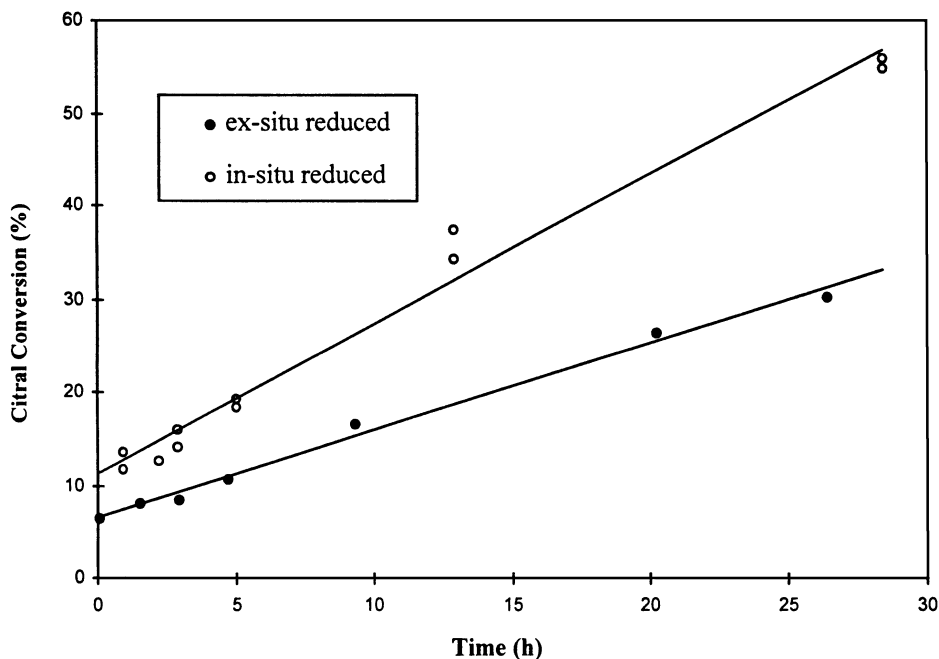


FIG. 4. Effect of pretreatment procedure for reaction over 1.44% Pt/SiO₂ catalyst at 373 K, 20 atm H₂ pressure, and 1 M citral in hexane. Catalyst amounts 0.50 and 0.80 g were used for the *in situ* and *ex situ* reduced catalysts, respectively.

rate of citral hydrogenation (citral conversions less than 20%) over a 2.65% Pt/SiO₂ catalyst at temperatures from 298 to 423 K, H₂ pressures from 7 to 41 atm, and citral concentrations from 0.97 to 5.9 mole/liter in hexane. The initial rate of citral hydrogenation was zero order and first order with respect to citral concentration and hydrogen pressure, respectively.

Figure 5 displays the temporal citral conversion profile for reaction under standard conditions using 1.44% Pt/SiO₂

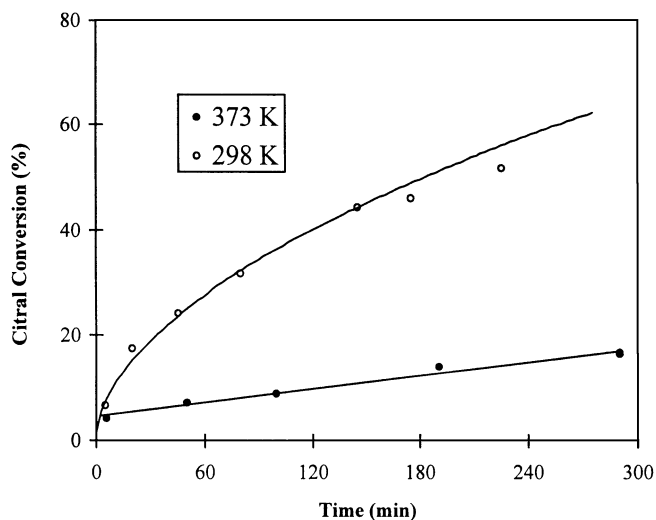


FIG. 5. Temporal citral conversion profile for reaction over 0.80 g of 1.44% Pt/SiO₂ catalyst at 298 and 373 K, 20 atm H₂, and 1 M citral in hexane.

at 298 and 373 K. The initial TOF for citral disappearance is 0.18 s⁻¹ at 298 K and 0.02 s⁻¹ at 373 K, which represents almost an order of magnitude decrease in the rate even though the reaction temperature is 75 K higher. However, the higher initial rate at 298 K is accompanied by strong deactivation, as shown in Fig. 6 where the instantaneous H₂ uptake profile is plotted as a function of citral conversion under standard conditions and 298, 373, and 423 K. The instantaneous TOF for H₂ uptake at 298 K with 0.8 g of catalyst decreased from 0.5 s⁻¹ during the first 10 min of reaction to 0.05 s⁻¹ after 4 h of reaction time and 50% citral conversion. Artifacts due to transport resistance and

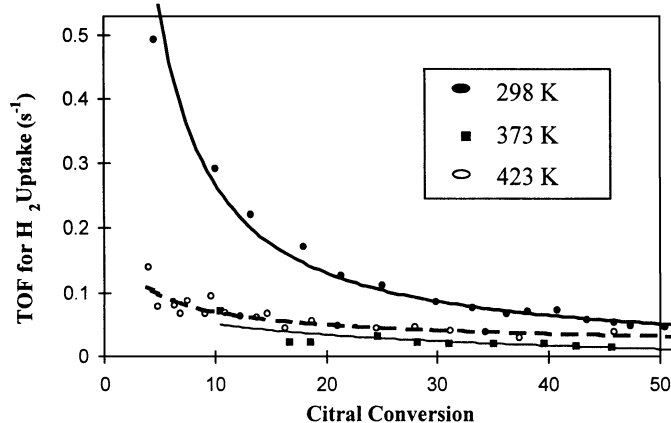


FIG. 6. TOF for H₂ uptake as a function of citral conversion for reaction over 1.44% Pt/SiO₂ at 298, 373, and 423 K at 20 atm H₂ and 1 M citral in hexane.

poisoning were discounted after application of the Madon–Boudart test, as shown in Fig. 2 and Table 2. Reaction with 0.5 g of 1.44% Pt/SiO₂ at 373 K yielded an initial TOF for H₂ uptake that was more than an order of magnitude lower than that at 298 K, but remained approximately constant as citral conversion increased. No H₂ uptake points were obtained for citral conversions less than 5% due to the fact that this level of citral conversion was obtained during the first few minutes of reaction, a period too short to allow quantitative analysis. The initial reaction rate decreased as the temperature increased from 298 to 373 K, but conventional Arrhenius behavior was seen during a further increase from 373 to 423 K with an activation energy of 7 kcal/mol. This is displayed in Fig. 6 which shows the instantaneous rate of H₂ uptake at 423 K is greater than that at 373 K. Similar to the reaction at 373 K, and in contrast to that at 298 K, negligible deactivation was observed at 423 K.

This unusual temperature effect on activity was accompanied by a dramatic change in product distribution, as shown in Figs. 7 and 8 for hydrogenation over 1.44% Pt/SiO₂ under standard conditions. Figures 7a and 8a show

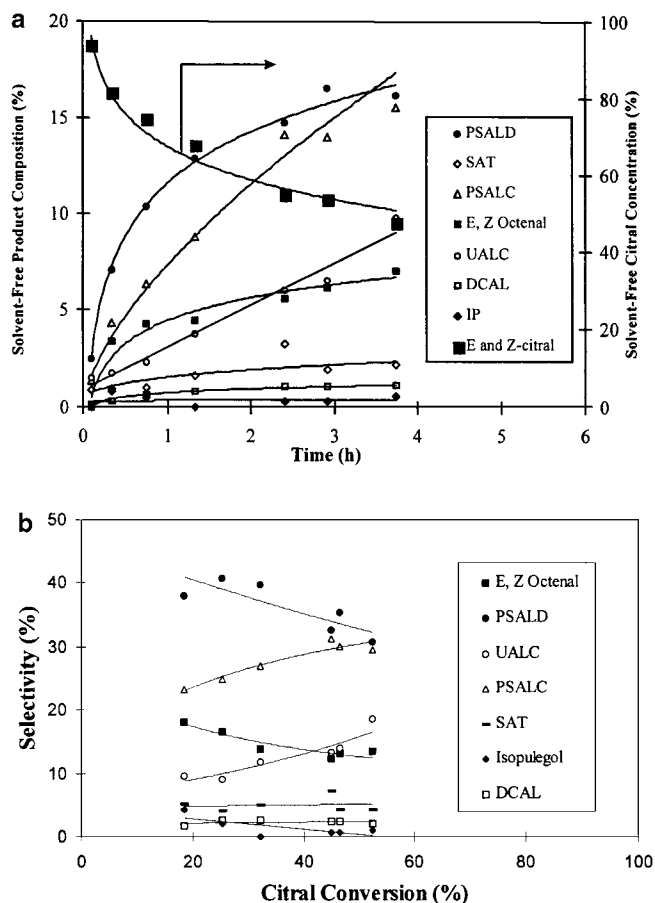


FIG. 7. (a) Concentration profile for reactants and products during citral hydrogenation over 1.44% Pt/SiO₂ at 298 K, 20 atm H₂ pressure, and 1 M citral in hexane. (b) Selectivity to reaction products as a function of citral conversion under the identical reaction conditions.

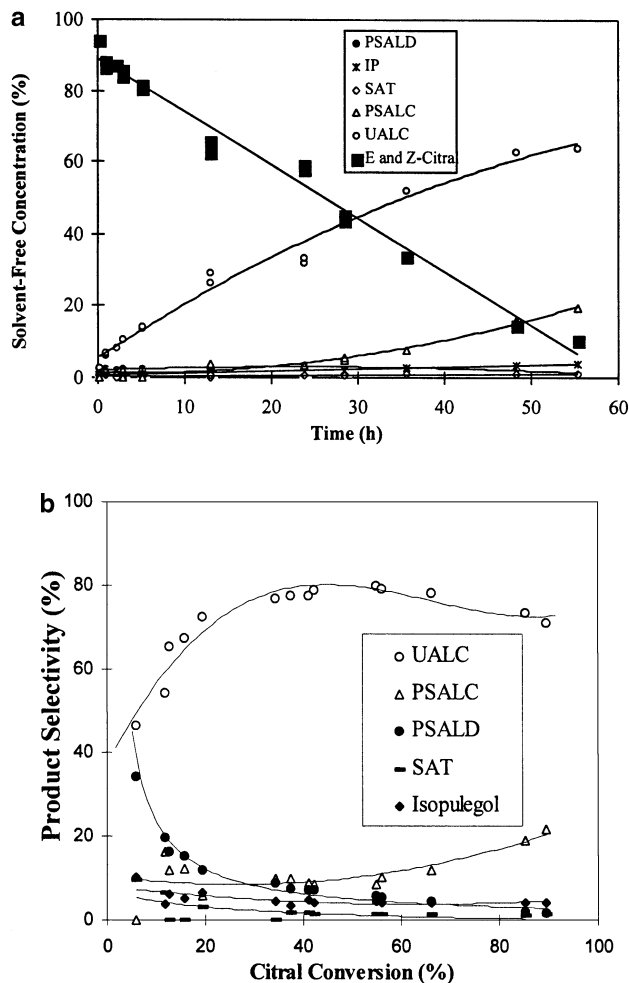


FIG. 8. (a) Concentration profile for reactants and products during citral hydrogenation over 1.44% Pt/SiO₂ at 373 K, 20 atm H₂ pressure, and 1 M citral in hexane. (b) Selectivity to reaction products as a function of citral conversion under identical reaction conditions.

the concentration profiles for reaction under standard conditions at 298 and 373 K, respectively. Consistent with the results in Fig. 5, the temporal concentration profile for citral at 298 K exhibits a sustained exponential-like decrease, with time, while a linear decrease, i.e., zero-order behavior, is observed for citral at 373 K (Fig. 8a). The concentrations of the *cis* and *trans* isomers of citral were summed and plotted in Figs. 7 and 8 since both isomers exhibit identical concentration dependencies and activation energies on Pt/SiO₂, although the TOF ratio between the *E* and *Z* isomers is 1.5. The selectivity to the UALC increases from 9 to 19% during the first 50% of citral conversion at 298 K, as contrasted with an increase from 40 to 80% for reaction at 373 K. The increase in selectivity to UALC at 373 K is accompanied by a decrease in the selectivity to the PSALD from approximately 40 to 5% during the first 50% conversion of citral. The selectivity to UALC decreases after 50% citral conversion at 373 K due to its further hydrogenation

TABLE 3

Effect of Reaction Temperature on Product Selectivity (mol%) during Reaction over 1.44% Pt/SiO₂ at 20 atm H₂ with 1 M Citral in Hexane: 30% Citral Conversion

Temperature (K)	UALC	IP	PSALC	PSALD	DCAL	SAT	ENAL
298	21	3	24	26	2	11	13
373	72	5	3	14	0	6	0
423	76	5	5	13	0	1	0

to PSALC. The selectivity to SAT at 373 K decreased as the citral conversion increased due to the fact that this product was formed only during the initial stages, and its concentration stayed constant with time even though the concentrations of other products increased. Thus, the numerator in Eq. [1] for SAT is constant with increasing citral conversion while the denominator increases with increasing citral conversion, resulting in a decrease in the cumulative selectivity to SAT with increasing citral conversion. For reaction at 298 K, on the other hand, the selectivity to PSALC and SAT increased with increasing citral conversion while the selectivity to IP decreased with increasing conversion. Table 3 lists the selectivities to the various products at 30% citral conversion for reaction over 1.44% Pt/SiO₂ under standard conditions and temperatures from 298 to 423 K. The high initial activity at 373 K during the first 5 min of reaction was associated primarily with the production of PSALD, and after this short period, the rate of formation of PSALD was suppressed while that for UALC increased.

More insight into this unique temperature behavior was obtained by performing a series of reactions under standard conditions with 1.44% Pt/SiO₂ and changing the temperature during the course of the reaction. Figures 9a and 9b depict the respective temporal citral conversion profiles for experiments in which the reaction was initially conducted at 373 K for 5 h prior to lowering the temperature to 298 K and vice versa. Figure 9a shows that decreasing the reaction temperature from 373 K, after 5 h of reaction and 17% citral conversion, to 298 K resulted in complete loss of activity. Figure 9b shows that the TOF at 298 K exhibited the usual decrease in the rate of citral disappearance and increasing the reaction temperature to 373 K resulted in a TOF for citral disappearance identical to that observed when the reaction was conducted at 373 K for the entire course of the reaction. The product distribution during the experiment where the reaction temperature was increased from 298 to 373 K midway through the reaction is displayed in Fig. 10. A drop in the selectivity to PSALD, SAT, and DCAL was accompanied by an increase in selectivity to UALC and PSALC after increasing the reaction temperature from 298 K during the first 4 h of reaction to 373 K.

Similar experiments were also conducted with 3.8% Pt/SiO₂ catalyst (H/Pt = 0.67) at temperatures between 373 and 423 K, and Figs. 11a and 11b display the temporal cit-

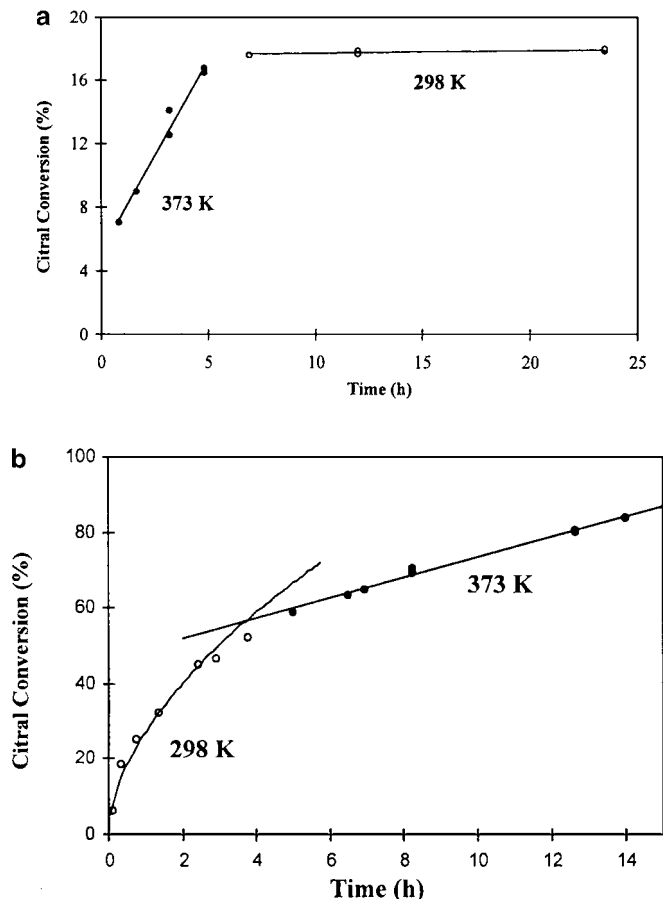


FIG. 9. (a) Temporal citral conversion profile during reaction over 1.44% Pt/SiO₂ (0.80 g) at 20 atm H₂ with 1 M citral in hexane (a) initially at 373 K prior to decreasing the reaction temperature to 298 K and (b) initially at 298 K prior to increasing to 373 K after 4 h of reaction.

ral conversion profiles for the reaction initially conducted at 373 K prior to increasing the reaction temperature to 423 K and vice versa. Increasing the reaction temperature from 373 to 423 K yielded a TOF of 0.04 s⁻¹ at 423 K

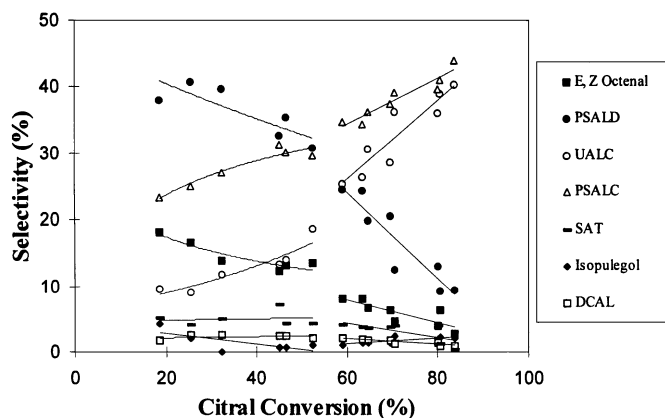


FIG. 10. Product distribution during the reaction initially at 298 K, 20 atm H₂, and with 1 M citral in hexane prior to increasing the reaction temperature to 373 K after 4 h of reaction and 50% citral conversion.

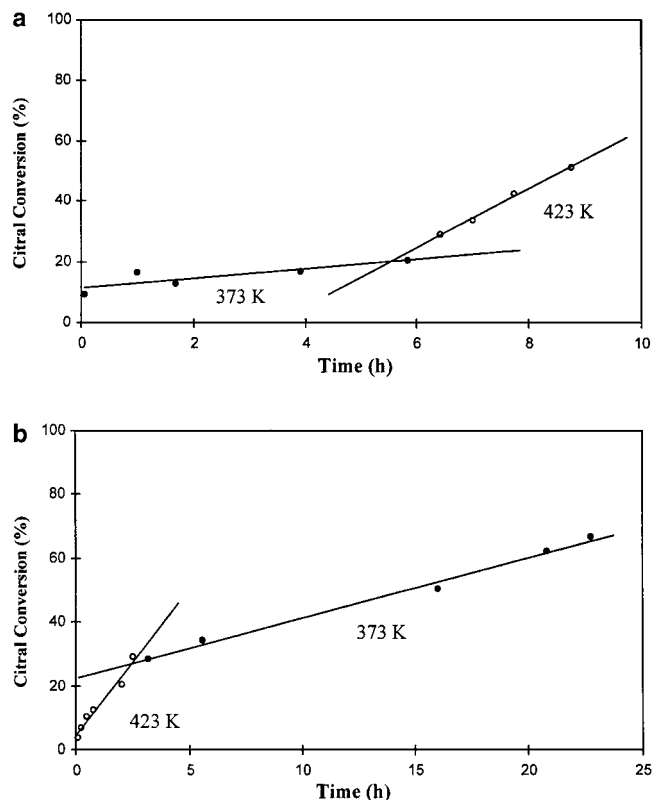


FIG. 11. (a) Temporal citral conversion profile during reaction over 3.8% Pt/SiO₂ (0.30 g) at 20 atm H₂ with 1 M citral in hexane (a) initially at 373 K prior to increasing to 423 K after 4 h of reaction and (b) initially at 423 K prior to decreasing to 373 K after 4 h of reaction.

which was identical to that obtained when the experiment was performed at 423 K for the entire course of the reaction. Similarly, decreasing the reaction temperature from 423 to 373 K yielded a TOF of 0.007 s⁻¹ at 373 K which was identical to that obtained when the reaction was conducted entirely at 373 K. The selectivity-versus-citral conversion profile obtained during these latter temperature experiments was similar to that exhibited when the reaction was performed in its entirety at each of the initial temperatures. The results of these experiments involving increasing and decreasing reaction temperature are summarized in Table 4. The observed rate of citral disappear-

TABLE 4

Relative Rates on 1.44% Pt/SiO₂ following a Sequence of Reaction Temperatures with 1 M Citral in Hexane and 20 atm H₂ Pressure^a

$T_{\text{initial}} \rightarrow T_{\text{final}}$	Relative rate
298 K \rightarrow 373 K	(Rate-373 K) _{final} /(rate-373 K) _{initial} = 1
373 K \rightarrow 298 K	(Rate-298 K) _{final} /(rate-298 K) _{initial} = 0
373 K \rightarrow 423 K	(Rate-423 K) _{final} /(rate-423 K) _{initial} = 1
423 K \rightarrow 373 K	(Rate-373 K) _{final} /(rate-373 K) _{initial} = 1

^aBased on Figs. 9 and 11.

ance at 373 and 423 K was retained regardless of the initial reaction temperature; however, there was no activity at 298 K when the initial reaction temperature was 373 K.

DISCUSSION

Influence of Mass Transfer and Poisoning Effects

It is imperative in liquid-phase reactions that heat and mass transfer effects as well as poisoning be shown to be absent. The Madon-Boudart test was conducted to discount artifacts due to heat and mass transfer limitations and poisoning on the measured kinetics of citral hydrogenation. It offers an efficient and reliable experimental technique for verifying the absence of heat and mass transfer limitations because the activity for a reaction is proportional to the number of active sites which, for a structure-insensitive reaction in the absence of poisoning effects, is proportional to the concentration of surface metal atoms (24). Previous studies had shown that no external mass transport limitations existed at stirring speeds above 500 rpm; all experiments here were conducted at 1000 rpm (23). The apparent structure sensitivity suggested for these types of reactions complicated the use of the Madon-Boudart test (26); however, this difficulty was overcome by using two catalysts with essentially equal dispersions of 0.41 and 0.45, as measured by H₂ chemisorption at 300 K. These two catalysts yielded similar TOFs at 373 and 393 K within experimental uncertainty (see Table 2), which indicated the absence of any transport limitations as well as poisoning effects due to impurities in the liquid phase. Furthermore, the constant turnover frequency for H₂ uptake at 298 K for catalysts with an order-of-magnitude variation in the concentration of surface Pt atoms and the identical temporal H₂ uptake curves at 298 K for an eightfold change in catalyst loading are further indications that these kinetic data are free of transport limitations and poisoning effects.

Since citral was used as received, with a purity of 97%, one must also be concerned about possible poisoning due to impurities in the reactant source. However, this was not a problem because a sixfold variation in citral concentration did not affect the activity or selectivity versus conversion behavior between 298 and 423 K, as indicated by the zero-order dependence of the initial rate on citral concentration (21). The difference in conversion between the runs at 298 K with an eightfold variation in catalyst loading (see Figs. 3a and 3b) is attributed to a concurrent inhibition by UALC, one of the intermediate products in the reaction, and not to poisoning effects. The possible leaching of metals from the reactor walls was also considered, but such an effect was discounted not only because catalyst poisoning by the leached metals would result in the Madon-Boudart criterion not being satisfied and the temporal H₂ uptake

curves for an eightfold variation in catalyst loading not being identical, but also because elemental analysis of hexane, used as a solvent for benzene hydrogenation, showed that the concentration of any leached metals on either the solid catalyst or in the liquid phase was below the detection limit (21, 23). Consequently, all experimental results, combined with utilization of the Weisz–Prater criterion, consistently verified the absence of artifacts due to internal or external diffusion limitations or to poisoning.

Effect of Pretreatment Procedure

The results in Fig. 4 clearly show that the pretreatment procedure can have a pronounced effect on the reaction rate because the catalyst reduced *ex situ* exhibited a TOF that was only one-third of that for the catalyst reduced *in situ*; however, the two different pretreatment procedures did not influence the product distribution. While treatment at 373 K in flowing H₂ is sufficient to reactivate a catalyst previously reduced at 673 K in hydrogen (27); the presence of solvent during the reactivation process may influence the state of the catalyst at the start of the reaction. Evidence of solvent effects during the reduction process was obtained by Busser *et al.*, who studied the reduction of polymer-stabilized Rh particles in various solvents and found the average metal particle size to vary fourfold depending on the nature of the solvent (28). Solvent effects during the reactivation process can also influence the catalyst by adsorbing competitively with hydrogen or by solvent decomposition (29). The lower TOF may also be due to the small amounts of oxygen present on the Pt surface and in the liquid feed that could form water, which may alter or block part of the catalyst surface. Although the oxygen concentration in the liquid phase is low, Augustine and Tanielyan have shown that oxygen dissolved in the solvent can modify the kinetics of ethyl pyruvate hydrogenation (20). Therefore, any complications that might arise from these effects were avoided by reducing the catalyst *in situ* and degassing citral and hexane with N₂ to remove any dissolved oxygen.

Effect of Reaction Temperature on Product Distribution

The conjugated functionality in citral may have considerable steric constraints imposed on its adsorbed state because of the methyl and long-chain aliphatic substituents that are not present in smaller molecules such as acrolein and crotonaldehyde. Steric constraints imposed on the conjugated C=C and the trisubstituted isolated C=C bonds should make hydrogenation of these functionalities more difficult. In fact Beccat *et al.* have shown by a comparison of crotonaldehyde and methylcrotonaldehyde that the presence of a methyl group in place of a hydrogen on the conjugated C=C functionality decreases the hydrogenation rate of the C=C bond fourfold and increases the rate of hydrogenation of the C=O bond 4-fold (6). These authors

did not consider the possible isomerization of unsaturated alcohol to saturated aldehyde; therefore, the relative rate enhancement for hydrogenation of the C=O bond may be even larger. Considering these arguments, it is surprising that, despite the steric constraints associated with the citral molecule, a 40% selectivity for hydrogenation of only the conjugated C=C bond to yield PSALD and a 15% selectivity for hydrogenation of the trisubstituted, isolated C=C bond to yield DCAL and SAT can be obtained at low citral conversions, i.e., less than 20%. The results are even more striking when one considers that no isomerization of UALC to PSALD was observed in the present study, even during hydrogenation of the pure intermediate feeds, i.e., geraniol and nerol (the *cis* and *trans* isomers of UALC). These results indicate that the conjugated bonds in citral participate in adsorption and that steric constraints, while present, do not play a dominant role in determining the product distribution over these unmodified clean Pt/SiO₂ catalysts. Coordination via the sterically hindered site was reported in a RAIRS study of crotonaldehyde adsorption on Pt(111) surfaces (30). However, steric constraints may come into play during the course of the reaction due to surface modification (31).

The product distribution during citral hydrogenation was strongly dependent on the reaction temperature. All results are under standard conditions unless otherwise noted. Reactions conducted at 373 and 423 K gave high selectivities to the primary products, i.e., UALC and PSALD, whereas hydrogenation at 298 K yielded numerous secondary products due to readsorption and further reaction of the primary products. This is evidenced by higher selectivity to PSALC and SAT at 298 K compared with 373 K (Figs. 7, 8). The selectivity to PSALD at 298 K was approximately 40% at 20% citral conversion and 30% at 50% citral conversion. In contrast, reaction at 373 K initially yielded a selectivity to PSALD of approximately 40%, which decreased to 10% after 20% citral conversion and to less than 5% after 50% citral conversion (Fig. 8b). The sharp decrease in the selectivity to PSALD at 373 K was due to its formation only during the first few minutes of reaction, after which period its net rate of formation was suppressed and the rate of UALC formation was enhanced. The selectivity to UALC at 298 K increased from 9 to 19% as the citral conversion increased from 20 to 50%; however, at 373 K the UALC selectivity increased from 40 to 80% as the citral conversion grew from 5 to 50%. Thus, it appears as though there is a surface modification that occurs under reaction conditions whose formation is suppressed at 298 K compared with 373 K.

Gallezot and co-workers observed similar changes in product distribution during liquid-phase hydrogenation of cinnamaldehyde over Pt and Ru catalysts. They suggested that both geometric and electronic effects induced by competitive hydrocinnamaldehyde (saturated aldehyde)

adsorption were responsible for the selectivity-versus-conversion behavior. The geometric effect was proposed to be due to the surface ligands imposing constraints on the adsorption of cinnamaldehyde such that adsorption only through the carbonyl bond was allowed, while the electronic effect involved donation of electrons from the ligands, thus increasing the electron density at the surface and inhibiting adsorption via the conjugated C=C bond (31). Lercher and co-workers have suggested that formation of butyraldehyde during liquid-phase hydrogenation of crotonaldehyde is accompanied by deactivation of sites responsible for butyraldehyde formation (19). This is in agreement with IR studies of 3-methyl-2-butenal which show that the formation of saturated aldehyde is accompanied by subsequent decarbonylation to yield adsorbed CO and carbonaceous deposits on the surface (32). Thus, several studies have suggested surface modifications occur under reaction conditions that can alter selectivity, and a majority of these studies have indicated that PSALD may be responsible for the modification. However, in view of the results in our subsequent article, the modification is attributed to UALC rather than PSALD (21).

It is worth noting that a number of bimetallic systems have been investigated for selective hydrogenation of α,β -unsaturated aldehydes, with the purpose of enhancing selectivity to the UALC, because it was thought that simpler monometallic catalysts such as Pt/SiO₂ exhibited a low selectivity to UALC. However, in view of the results presented in this paper, it is apparent that the effect of reaction parameters on product distribution can be significant and can alter the selectivities as much or more than the addition of a second metal.

Deactivation Process via Inhibition

There is more than an order of magnitude drop in the reaction rate during the first 4 h of reaction at 298 K, as shown in Fig. 3. This deactivation process cannot be attributed to transport limitations or poisoning effects, as discussed before. Figures 3a and 3b show that, despite an eightfold difference in catalyst loading, the temporal H₂ uptake curves are identical while the H₂ uptake-versus-citral conversion profiles are significantly different. Such behavior is consistent with a concurrent side reaction yielding inhibiting products that accumulate on the catalyst surface on the time scale of the reaction (21). If the reaction were zero order with no inhibition reaction, then the temporal TOF profile and the TOF-versus-conversion profile would be identical for the two runs with an eightfold different catalyst loading. The identical TOF-versus-time profile in Fig. 3a is exhibited because the *fraction* of sites occupied by the inhibiting species is identical for the two runs with different catalyst loading, and therefore, the turnover frequency is constant with time. However, due to the inhibition reaction the total number of sites available for reaction at each point in time

in greater, and hence citral conversion is greater, for the reaction with the greater catalyst mass (21). The source of the inhibition reaction was believed to be a decomposition of UALC. A number of studies have been reported in the literature that have shown the existence of decomposition reaction for such systems yielding chemisorbed CO and carbonaceous species (31–33). Furthermore, the work of Lercher and co-workers for liquid-phase hydrogenation of crotonaldehyde indicated that purging a deactivated catalyst with air to oxidize CO to CO₂ regenerated the initial hydrogenation activity that was observed prior to deactivation (19).

Effect of Temperature on Reaction Rate

As illustrated in Fig. 6, an activity minimum is observed between 298 and 423 K which occurred over the entire pressure range of 7 to 20 atm. Lercher and co-workers have reported a decreasing reaction rate with increasing temperature for crotonaldehyde hydrogenation (19); however, to our knowledge, an activity minimum for this or any other liquid-phase hydrogenation reaction has not been reported in the literature. An activity maximum, on the other hand, has been frequently reported for vapor-phase hydrogenation reactions, and it can be readily attributed to the competition between an increasing rate constant and a decreasing adsorption equilibrium constant as the temperature increases (34, 35). This explanation cannot explain an activity minimum, however. Lercher and colleagues have suggested that the activity decrease with increasing temperature is due to decarbonylation of butyraldehyde occurring concurrently with crotonaldehyde hydrogenation, and they speculated that the former reaction may have a higher activation energy compared with the latter reaction; thus the relative inhibition due to site blockage would increase at higher reaction temperatures (19). Regardless, this mechanism alone is not capable of explaining either an activity minimum or the differences in deactivation behavior observed at the different temperatures in the present study.

We propose that the activity minimum is caused by the decomposition of UALC combined with CO desorption. Our choices for the reactant that decomposes are nerol and geraniol, rather than an aldehyde suggested in previous studies (19, 30, 32). This conclusion is based on the results discussed in the subsequent paper (36). Briefly, these data indicate zero-order behavior for hydrogenation of pure PSALD at 298 and 373 K with little deactivation, which contrasts noticeably with the sharp decrease in the rate observed during UALC hydrogenation at 298 and 373 K. Furthermore, simultaneous hydrogenation of PSALD and UALC resulted in a continuous decrease in the rate of disappearance of PSALD in contrast to the stable rate obtained for hydrogenation of PSALD alone, which strongly suggests a deactivation phenomenon due to UALC (36). Further indirect evidence for UALC as the source of CO

lies in the fact that citral hydrogenation at 373 K initially occurs at a very high reaction rate which rapidly decreases to a pseudo-steady-state behavior as soon as UALC is formed. It is possible that citral decomposition may also play a role in inhibition and such a reaction cannot be discounted based on the results presented in the present study; nevertheless, a decomposition reaction is believed to occur under the present reaction conditions. The CO formed from this reaction begins to desorb at higher reaction temperatures, i.e., 373 K and above. TPD studies of aldehyde and alcohol decomposition on Pd and Rh as well as ketene decomposition on single-crystal Pt surfaces indicate that the decarbonylation product, CO, begins to desorb from the surface at 350 K, with a peak maximum around 450 K (33, 37–44).

At 298 K, CO desorption from Pt essentially does not occur; therefore, the reaction rate gradually decreases with time due to buildup of adsorbed CO on the time scale of the reaction, eventually leading to complete loss of activity (Figs. 6, 7a, 9a). Increasing the temperature to 373 K results in the rate enhancement for both the alcohol decomposition and CO desorption processes, and a pseudo-steady state is readily established for the CO coverage on Pt which results in a stable activity during reaction at 373 K. Furthermore, normal Arrhenius behavior is observed between 373 and 423 K (Figs. 6, 11) since the desorption rate of CO is high and a steady-state Pt surface with a lower CO coverage is again rapidly obtained. Such a mechanism would imply that the activation barrier for decomposition reaction should be lower than that for CO desorption. Indeed, BOC theory estimates of the activation barrier associated with decarbonylation of acetyl species, which have been proposed as intermediates in alcohol decomposition, range from 15 to 26 kcal/mol depending on the mechanism (21, 45), while the activation barrier for CO desorption from Pt(111) surfaces has been reported to be approximately 26 kcal/mol (46, 47). The activation barrier estimated for decomposition on Pt surfaces is consistent with the value of 16 kcal/mol obtained for propenyl decomposition on a Pd(111) surface (36). The mechanism of the decomposition reaction is discussed in greater detail later; however, it is important to emphasize that the activity minimum can be explained by the relative activation barriers for alcohol decomposition and CO desorption.

Kinetic Modeling

The mechanism proposed above would suggest the presence of a hydrocarbon with one carbon atom less than UALC, and evidence for this species in trace quantities was obtained via GC-MS; however, analytical limitations prevented resolution of this species in our gas chromatograms (21). The reaction sequence proposed previously and shown in Fig. 1 was modeled via a Langmuir–Hinshelwood mechanism for each hydrogenation step along with a sequence of irreversible steps to account for alcohol decomposition

and CO desorption. It was implicitly assumed in the model that the concentrations of products arising from the alcohol decomposition reaction, i.e., organic fragment and CO, are very small.

Reactions 1–5 in Fig. 1 are the principal ones in our system and were modeled using the following five mole balances for the species of interest:

$$\frac{dC_{\text{CITRAL}}}{dt} = -r_1 - r_2 - r_3, \quad [2a]$$

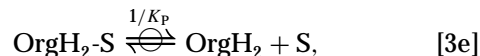
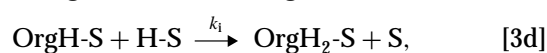
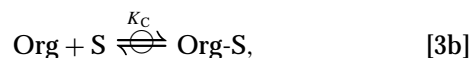
$$\frac{dC_{\text{ENAL}}}{dt} = r_1, \quad [2b]$$

$$\frac{dC_{\text{UALC}}}{dt} = r_2, \quad [2c]$$

$$\frac{dC_{\text{PSALD}}}{dt} = r_3 - r_5, \quad [2d]$$

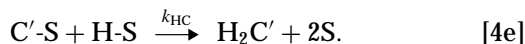
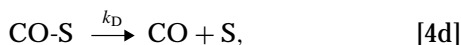
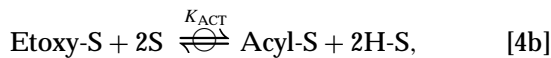
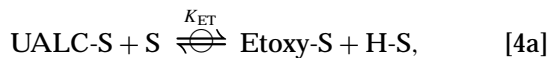
$$\frac{dC_{\text{PSALC}}}{dt} = r_5, \quad [2e]$$

where C_i and r_j are the concentration of species i and reaction rate of step j in Fig. 1, respectively. Equations [2c] and [2e] were formulated based on the assumption that hydrogenation of geraniol to citronellol, i.e., r_4 , is kinetically insignificant under citral hydrogenation reaction conditions. This was verified experimentally as shown in the subsequent paper by addition of either geraniol or citronellal to a 1 M citral in hexane hydrogenation reaction mixture at 373 K. Addition of geraniol resulted in negligible change in the net rates of formation and disappearance of geraniol and citronellol, respectively. Addition of citronellal, on the other hand, to a similar reaction mixture resulted in a significant enhancement in the net rate of disappearance of citronellal and formation of citronellol and isopulegol (36). Therefore, the primary route to citronellol formation appears to be via citronellal hydrogenation. Only the organic species listed above were used in this simplified model because they constitute approximately 95% of the total products (Figs. 7, 8). An identical sequence of elementary steps comprising a simple Langmuir–Hinshelwood model describes each of the reactions in steps 1–5, i.e.,



where Org is the organic reactant, i.e., citral in reactions 1, 2, and 3 and PSALD in reaction 5. The terms S, Org-S, OrgH-S, OrgH₂-S, and H-S represent vacant active sites, adsorbed organic, adsorbed half-hydrogenated organic species, adsorbed product, and adsorbed hydrogen, respectively.

In addition to the above sequence of steps for each hydrogenation reaction, it was also assumed that there is a concurrent inhibiting mechanism due to decarbonylation of UALC to yield adsorbed CO and carbonaceous deposits as follows:



The first step is the quasi-equilibrated dissociation of UALC to yield a surface ethoxide species and adsorbed hydrogen. The surface ethoxide species then dehydrogenates to form an acyl species (30), which subsequently undergoes C-C bond scission to yield adsorbed CO and a carbonaceous species with one carbon atom less than UALC. The adsorbed CO can desorb and the carbonaceous species can hydrogenate with rate constants k_{D} and k_{HC} , respectively. The details of the mechanism and generalizations based on other metals are discussed later.

Assuming adsorption of the reactants and formation of the half-hydrogenated species are quasi-equilibrated, the following respective expressions are obtained for the surface coverage of hydrogen, the organic, and the half-hydrogenated state:

$$\Theta_{\text{H}} = K_{\text{H}_2}^{1/2} P_{\text{H}_2}^{1/2} \Theta_{\text{S}}, \quad [5a]$$

$$\Theta_{\text{Org}} = K_{\text{Org}} C_{\text{Org}} \Theta_{\text{S}}, \quad [5b]$$

$$\Theta_{\text{OrgH}} = K_{\text{li}} \Theta_{\text{Org}} \frac{\Theta_{\text{H}}}{\Theta_{\text{S}}} = K_{\text{li}} K_{\text{Org}} K_{\text{H}_2}^{1/2} P_{\text{H}_2}^{1/2} C_{\text{Org}} \Theta_{\text{S}}, \quad [5c]$$

$$\begin{aligned} \Theta_{\text{ACYL}} &= K_{\text{ACT}} \frac{\Theta_{\text{ETOXY}} \Theta_{\text{S}}^2}{\Theta_{\text{H}}^2} \\ &= K_{\text{ACT}} K_{\text{H}_2}^{-3/2} P_{\text{H}_2}^{-3/2} K_{\text{ET}} K_{\text{UALC}} C_{\text{UALC}} \Theta_{\text{S}} \\ &= K'_{\text{ACT}} C_{\text{UALC}} \Theta_{\text{S}}, \end{aligned} \quad [5d]$$

where K_i and C_i are the adsorption equilibrium constant and concentration of species i , respectively, and K_{li} and K'_{ACT} are the equilibrium constant for formation of the half-hydrogenated species and a lumped apparent equilibrium constant for formation of the acyl species, respectively. If the addition of the second H atom is assumed to be the rate-determining step, then the rate of the hydrogenation reaction in Fig. 1 for component i is

$$r_i = L k_i K_{\text{li}} K_{\text{Org}} K_{\text{H}_2} P_{\text{H}_2} C_{\text{Org}} \Theta_{\text{S}}^2 = \alpha_i C_{\text{Org}} \Theta_{\text{S}}^2, \quad [6]$$

where the subscript Org represents the organic reactant in each step and L is the concentration of active sites. Note

that P_{H_2} remains constant during reaction and is therefore lumped into the constant α . Using the site balance along with the assumptions that Θ_{H} , Θ_{PSALD} , Θ_{UALC} , and $\Theta_{\text{C}} \ll \Theta_{\text{Citral}}$ and Θ_{CO} , the following expression for the fractional surface coverage of sites is obtained:

$$\begin{aligned} \Theta_{\text{Citral}} + \Theta_{\text{S}} + \Theta_{\text{CO}} &= 1, \\ \Theta_{\text{S}} &= \frac{1 - \Theta_{\text{CO}}}{1 + K_{\text{Citral}} C_{\text{Citral}}}; \end{aligned} \quad [7]$$

and the resulting rate expression is

$$r_i = \frac{k'_i K_{\text{li}} K_{\text{Org}} K_{\text{H}_2} P_{\text{H}_2} C_{\text{Org}} (1 - \Theta_{\text{CO}})^2}{(1 + K_{\text{Citral}} C_{\text{Citral}})^2}, \quad [8]$$

where L is incorporated into the rate constant k'_i . Furthermore, using the inhibition process controlled by reactions involving UALC decarbonylation and CO desorption, shown in steps 14a–14e, the following differential equation for the surface coverage of CO can be obtained after using step 15d:

$$\begin{aligned} \frac{d\Theta_{\text{CO}}}{dt} &= k_{\text{ACT}} \Theta_{\text{ACYL}} \Theta_{\text{S}} - k_{\text{D}} \Theta_{\text{CO}}, \\ \frac{d\Theta_{\text{CO}}}{dt} &= \frac{k_{\text{ACT}} (K_{\text{ACT}} K_{\text{ET}} K_{\text{UALC}}) C_{\text{UALC}} \Theta_{\text{S}}^5}{K_{\text{H}}^{3/2} P_{\text{H}_2}^{3/2} \Theta_{\text{S}}^3} - k_{\text{D}} \Theta_{\text{CO}}, \\ \frac{d\Theta_{\text{CO}}}{dt} &= k'_{\text{CO}} C_{\text{UALC}} \Theta_{\text{S}}^2 - k_{\text{D}} \Theta_{\text{CO}}. \end{aligned} \quad [9]$$

Therefore, our kinetic model consists of Eq. [8] and six differential equations comprising Eqs. [2a]–[2e] and [9] subject to the initial conditions that $C_{\text{Citral}} = 1$ M, $C_{\text{Org}} = 0$ for all reactants other than citral and $\Theta_{\text{CO}} = 0$. These equations were solved numerically with six adjustable parameters, i.e., four lumped constants, α_1 – α_3 and α_5 , and the adsorption equilibrium constant for citral and the apparent rate constant for CO dissociation, k'_{ACT} . The value for k_{D} was calculated using results from the surface science literature, i.e., $k_{\text{D}} = 10^{13} * e^{-26,000/RT}$ (46). The numbers of data points used for fitting purposes at 298, 373, and 423 K are 30, 44, and 32, respectively. Admittedly, this model requires a large number of adjustable parameters; however, they are essential to accurately account for the complex reaction chemistry. Parameter estimation was performed using the Powell method via a commercially available non-linear regression software package named Scientist (Micro Math Scientific Software) which has a tolerance of 10^{-6} . The optimum fit of the above model to the concentration profiles under standard conditions and 298, 373, and 423 K is shown in Fig. 12, and the corresponding parameters are listed in Table 5. When possible, the thermodynamic consistency of these values was examined, as discussed later. All the fitting was performed at a reactor pressure of 20 atm; therefore, the adsorption equilibrium constant and the

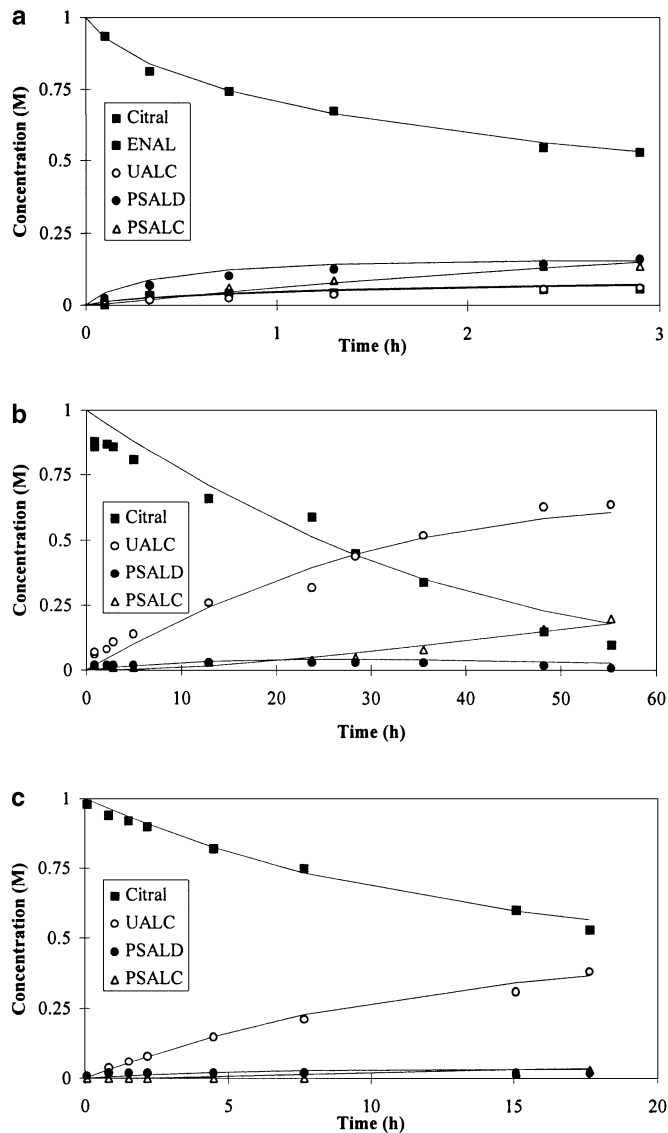


FIG. 12. Fit of kinetic model to experimental data for reaction over 1.44% Pt/SiO₂ at 20 atm H₂ with 1 M citral in hexane at (a) 298 K, (b) 373 K, and (c) 423 K. Symbols represent experimental data while solid lines represent the model prediction.

partial pressure of hydrogen were lumped in with other constants.

Prior to discussing the modeling results it is important to address the various assumptions involved. The model was restricted to the consideration of reactions 1–3 and 5 at 298 K because the products of these five reactions constituted 95% of the total products, and at 373 and 423 K only reactions 2, 3, and 5 were considered because the concentration of ENAL was negligible at these temperatures. Dissociative hydrogen adsorption on Pt is well established (48, 49). A single type of active site was used, i.e., one that can adsorb hydrogen as well as the organic molecules; such an assumption is routinely made for these types of hydrogenation reactions and is the simplest choice possible. The first-order dependence on H₂ implies a low surface coverage of H atoms. The addition of the second H atom as the rate-determining step (rds) has been proposed previously for the vapor-phase hydrogenation of ketones and aldehydes on metal surfaces (50, 51). This assumption allows first-order dependence on hydrogen pressure, as observed experimentally, in contrast to a maximum half-order dependency that is predicted if addition of the first H atom is assumed to be the rds.

The rate inhibition caused by site blockage due to CO, as represented by steps 4a–4e, was invoked to explain the unusual temperature dependence. The need for such a postulate has been discussed previously; therefore, we now concentrate on the chemistry involved in these steps. Much evidence exists that clearly shows that decomposition of saturated aldehydes and unsaturated alcohols does occur; consequently, all these species may undergo a surface decomposition reaction to different extents under our reaction conditions. However, only the decomposition of UALC is considered here based on the reasons summarized earlier and more clearly enumerated in a subsequent paper (21).

The elementary decomposition reactions proposed in the present model are consistent with the work of Barteau and co-workers for alcohols on Pd surfaces (52, 53). Recently, Carlos de Jesus and Zaera have confirmed that decarbonylation of acrolein and crotonaldehyde does indeed occur on

TABLE 5
Optimized Parameters for Eqs. [2], [8], and [9]

	423 K	373 K	298 K	E_a or ΔH_{ads}^0 (kcal/mol)	$\ln(A_0)$ or ΔS_{ads}^0 (cal/mol/K)
$\alpha_1 = k_1' K_{11} K_{\text{Citral}} K_{\text{H}_2} P_{\text{H}_2}$ (h ⁻¹)	0.00	0.00	23.66		
$\alpha_2 = k_2' K_{12} K_{\text{Citral}} K_{\text{H}_2} P_{\text{H}_2}$ (h ⁻¹)	1.50	27.63	26.06		
$\alpha_3 = k_3' K_{13} K_{\text{Citral}} K_{\text{H}_2} P_{\text{H}_2}$ (h ⁻¹)	0.28	8.47	105.24		
$\alpha_5 = k_5' K_{15} K_{\text{PSALD}} K_{\text{H}_2} P_{\text{H}_2}$ (h ⁻¹)	4.86	89.35	354.87		
K_{Citral} (liters/mol)	4.60	15.98	20.14	-19 ^a	-36 ^a
k_{CO} (liters/mol/h)	138216	62926	4887	8	21
k_{D} (h ⁻¹)	1303.00	20.50	0.003	26 ^b	38 ^b

^a Enthalpies and entropies of adsorption were evaluated at a standard state of 1 atm in the gas phase.

^b Value was fixed based on estimates from the literature (46, 47).

Pt surfaces to yield CO and volatile carbonaceous species (31, 54). Unfortunately, similar detailed studies regarding decomposition pathways of unsaturated alcohols on Pt surfaces were not found and, therefore, the justification of the present model is based heavily on studies with Pd. TPD studies of allyl alcohol adsorption on a Rh(111) surface indicate desorption of CO, hydrogen, and allyl alcohol, and no C₂ hydrocarbons could be detected (42). In contrast, similar studies of Pd(110) yielded CO, hydrogen, ethylene, propanal, ethane, and allyl alcohol (33), while studies with a Pd(111) surface identified hydrogen, CO, propylene, ethylene, and water, which is indicative of C–O bond cleavage and suggestive of an apparent structure sensitivity for alcohol decomposition on Pd surfaces (37, 52). In view of these results, one must be careful about making broad generalizations regarding details of the decomposition reaction from one metal to another. Furthermore, Rendulic and Sexton compared their dehydrogenation results under UHV conditions with those on a supported Pt catalyst and concluded that extreme caution must be used in comparing data from UHV conditions with those relevant at higher pressures (55). Nevertheless, it is apparent that such side reactions do occur on Group VIII metal surfaces and the general results can be used to explain the unusual temperature behavior. Therefore, for the purposes of the present study the decomposition pathway of the unsaturated alcohol on Pt catalysts was assumed to be similar to that on Pd surfaces. Alcohol decomposition on Pd surfaces is believed to occur via an aldehyde intermediate to yield a surface acyl species which subsequently undergoes C–C bond scission to yield CO and carbonaceous species (53, 56); consequently, a similar mechanism is proposed for UALC decomposition in the present study. This raises the question that if the unsaturated alcohol decomposition occurs via an aldehyde intermediate then what precludes the initial unsaturated aldehyde i.e., citral, from also undergoing a decarbonylation reaction. This issue is addressed in the subsequent paper (36); however, at this point citral decarbonylation cannot be discounted although it is our assertion that the unsaturated alcohol forms a precursor prior to decarbonylation to yield CO and carbonaceous species. Furthermore, this precursor is speculated to be an acyl surface intermediate based on the surface science studies of Davis and Barteau (56).

Davis and Barteau studied aldehyde decomposition on Pd(111) and concluded that decomposition of an acyl species via a ketene intermediate was the rate-determining step rather than cleavage of the aldehydic C–H bond, and the activation energy for the former step was estimated to be 16 kcal/mol during decomposition of propenoyl (39). This is in general agreement with the trends for activation barriers obtained from bond-order conservation theory for a Pt(111) surface which indicates activation barriers of 13 kcal/mol for cleavage of the aldehydic carbon-

hydrogen bond and 26 kcal/mol for cleavage of the C–H bond in a surface acetyl species to form adsorbed ketene (21, 46). An alternate reaction pathway was proposed by Barteau and co-workers for decomposition of acetaldehyde on a Pd(110) surface in which the aldehydic hydrogen was cleaved to form a surface acetyl species which subsequently decomposed to CO and CH₃ without going through the ketene intermediate (41). The apparent structure sensitivity of the decomposition reaction does not allow us to say unequivocally which reaction occurs; therefore, for the sake of simplicity the acyl species has been assumed to decarbonylate to yield CO and an alkyl species. The activation barrier for this step on Pt(111) surfaces was estimated from bond-order conservation theory to be 15 kcal/mol (21). The observed minimum in activity can, in principle, be explained using either of the two mechanisms proposed by Barteau and co-workers as long as each activation barrier is lower than that for CO desorption. It is also possible that the apparent structure sensitivity seen during decomposition of aliphatic aldehydes and alcohols on Pd surfaces may be related to the apparent structure sensitivity observed for citral hydrogenation during reaction at 373 K over Pt/SiO₂ catalysts as shown in Table 1 (41, 52, 57).

The reverse of the acyl decomposition reaction is similar to the hydroformylation reaction; thus, acyl decomposition can, in principle, be a reversible reaction. However, this step was chosen to be irreversible since it is expected that the alkyl species should rapidly hydrogenate and the very low CO pressure would make the reverse reaction rate extremely slow. Evidence in the surface science literature suggests high selectivity toward hydrogenation of the carbonaceous deposits to form saturated and unsaturated alkyl species rather than the formation of alkylidyne species on the surface. Shekhar and Barteau have reported a selectivity of 88% for C₂ hydrocarbon products during decomposition of allyl alcohol in the presence of hydrogen, as opposed to 67% in the absence of hydrogen. In both cases C₂ species desorbed below 300 K (33); therefore, it is logical to assume that the surface coverage of these species is negligible.

The kinetic model just discussed adequately describes the experimental data and is consistent with observations reported by numerous workers. Furthermore, the fitted parameters yield thermodynamically consistent parameters when such evaluation is possible. The thermodynamic constraints on the equilibrium adsorption constants have been described before along with the proper choice of standard states (58, 59). Only the adsorption equilibrium constants for citral and UALC could be evaluated because the other parameters were coupled in such a manner as to disallow extraction of the equilibrium constants. Table 5 lists the fitted values of the adjustable parameters and the thermodynamic parameters obtained from the Arrhenius plots. The enthalpies and entropies of adsorption have been corrected to a standard state of 1 atm in the gas phase by a procedure

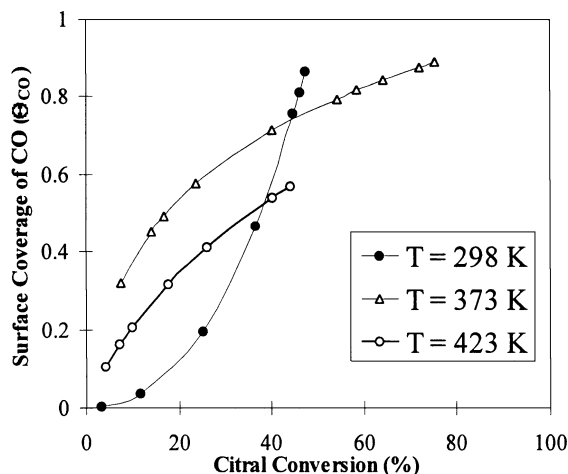


FIG. 13. Prediction of CO surface coverage as a function of citral conversion for reaction at 20 atm H₂ with 1 M citral in hexane at 298, 373, and 423 K using Eqs. [2], [8], and [9] with parameters in Table 5.

described earlier (23). Due to the large number of fitting parameters in the model, only a limited analysis of the resulting fitting parameters is possible. The enthalpy of citral adsorption was evaluated to be -19 kcal/mol, which is quite reasonable, and the entropy loss of 36 e.u. during citral adsorption was well below the absolute entropy of 83 e.u. calculated for citral in the gas phase at 298 K (21, 58, 59, 60).

The model described above was used to predict the surface coverage of CO under standard reaction conditions at 298, 373, and 423 K, and the results are shown in Fig. 13. It should be stressed that only relative comparison of the surface coverage at different reaction temperatures should be undertaken. The surface coverage of CO at 298 K starts out slowly but eventually reaches 0.9 at 50% citral conversion. At 10% citral conversion, the surface coverage of CO at 373 K is an order of magnitude higher than that at 298 K, which is consistent with our assertion that the lower reaction rate at 373 K is due to blockage of active sites by CO. Furthermore, at 10% conversion the surface coverage of CO at 423 K is lower than that at 373 K because of the enhanced CO desorption rate at this temperature, and conventional Arrhenius behavior is observed above 373 K.

SUMMARY

Citral hydrogenation was studied under kinetic conditions free of transport limitations and poisoning effects. The rate of citral hydrogenation exhibited a minimum in activity between 298 and 423 K, and this is attributed to the relative activation energies for the decomposition of the unsaturated alcohol and desorption of CO. At low reaction temperatures, i.e., 298 K, the rate of citral disappearance is low and CO slowly accumulates under reaction conditions to block active sites and eventually lead to a complete loss

of activity. At higher reaction temperatures, i.e., 373 K, alcohol decomposition is more rapid, but the CO desorption rate is significantly enhanced and a pseudo-steady state is readily established which results in minimal additional inhibition and conventional Arrhenius behavior with an activation energy of 7 kcal/mol. The reaction kinetics for each hydrogenation reaction in the reaction network were modeled using a Langmuir-Hinshelwood model invoking dissociative adsorption of hydrogen, competitive adsorption between hydrogen and the reactive organic species, and addition of a second H atom as the rate-determining step, and the observed product distributions at each temperature were described very well. Furthermore, deactivation due to decomposition of the unsaturated alcohols geraniol and nerol, along with CO desorption at higher temperatures, was invoked to account for the unusual rate dependence on temperature.

ACKNOWLEDGMENT

This study was supported by the DOE, Division of Basic Energy Sciences, under Grant DE-FE02-84ER13276.

REFERENCES

- Sheldon, R. A., *J. Mol. Catal. A* **107**, 75 (1996).
- Mercadante, L., Neri, G., Milone, C., Donato, A., and Galvagno, S., *J. Mol. Catal.* **105**, 93 (1996).
- Gallezot, P., and Richard, D., *Catal. Rev. Sci. Eng.* **40**, 81 (1998).
- Ponec, V., *Appl. Catal. A* **149**, 27 (1997).
- Kulson, P., and Cerveny, L., *Appl. Catal. A* **128**, 13 (1995).
- Beccat, P., Bertolini, J. C., Gauthier, Y., Massardier, J., and Ruiz, P., *J. Catal.* **126**, 451 (1990).
- Vannice, M. A., and Sen, B., *J. Catal.* **115**, 65 (1989).
- Patil, A., Banares, M. A., Lei, X., Fehlner, T. P., and Wolf, E., *J. Catal.* **159**, 458 (1996).
- Birchem, T., Pradier, C. M., Berthier, Y., and Cordier, G., *J. Catal.* **146**, 503 (1994).
- Coq, B., Figueras, F., Geneste, P., Moreau, C., Moreau, P., and Warawdekar, M., *J. Mol. Catal.* **78**, 211 (1993).
- Marinelli, T. B. L. W., Nabuurs, S., and Ponec, V., *J. Catal.* **151**, 431 (1995).
- Marinelli, T. B. L. W., and Ponec, V., *J. Catal.* **156**, 51 (1995).
- Touroude, R., *J. Catal.* **65**, 110 (1980).
- Birchem, T., Pradier, C. M., Berthier, Y., and Cordier, G., *J. Catal.* **161**, 68 (1996).
- Galvagno, S., Milone, C., Donato, A., Neri, G., and Pietropaolo, R., *Catal. Lett.* **17**, 55 (1993).
- Neri, G., Mercadante, L., Milone, C., Pietropaolo, R., and Galvagno, S., *J. Mol. Catal. A* **108**, 41 (1996).
- Neri, G., Milone, C., Donato, A., Mercadante, L., and Visco, A. M., *J. Chem. Technol. Biotechnol.* **60**, 83 (1994).
- Englisch, M., Ranade, V. S., and Lercher, J. A., *J. Mol. Catal.* **121**, 69 (1997).
- Englisch, M., Ranade, V. S., and Lercher, J. A., *Appl. Catal. A* **163**, 111 (1997).
- Augustine, R. L., and Tanielyan, S. K., *J. Mol. Catal. A* **118**, 79 (1997).
- Singh, U. K., Ph.D. thesis, Pennsylvania State University, in progress.
- Palmer, M. B., and Vannice, M. A., *J. Chem. Technol. Biotechnol.* **30**, 205 (1980).
- Singh, U. K., and Vannice, M. A., *AIChE J.* **45**, 1059 (1995).

24. Madon, R. J., and Boudart, M., *Ind. Eng. Chem. Fundam.* **21**, 438 (1982).
25. Satterfield, C. N., "Mass Transfer in Heterogeneous Catalysis," Robert E. Krieger, New York, 1981.
26. Englisch, M., Jentys, A., and Lercher, J. A., *J. Catal.* **166**, 25 (1997).
27. Coq, B., Crabb, E., Warawdekar, M., Bond, G. C., Slaa, J. C., Galvagno, S., Mercadante, L., Ruiz, J. G., and Sierra, M. C. S., *J. Mol. Catal.* **92**, 107 (1994).
28. Busser, G. W., van Ommen, J. G., and Lercher, J. A., "Advanced Catalysts and Nanostructured Materials." Academic Press, San Diego, 1996.
29. Mallat, T., Bodner, B., Borszky, K., and Baiker, A., *J. Catal.* **168**, 183 (1997).
30. Carlos de Jesus, J., and Zaera, F., *Surf. Sci.* **430**, 99 (1999).
31. Gallezot, P., Giroir-Fendler, A., and Richard, D., in "Chemical Industry 47" (Catalysis of Organic Reactions) (W. E. Pascoe, Ed.), 1992.
32. Waghay, A., and Blackmond, D. G., *J. Phys. Chem.* **97**, 6002 (1993).
33. Shekhar, R., and Barateau, M., *Surf. Sci.* **319**, 298 (1994).
34. Chou, P., and Vannice, M. A., *J. Catal.* **107**, 129 (1987).
35. Chou, P., and Vannice, M. A., *J. Catal.* **107**, 140 (1987).
36. Singh, U. K., Sysak, M., and Vannice, M. A., *J. Catal.* **190**, (2000).
37. Davis, J. L., and Barteau, M., *J. Mol. Catal.* **77**, 109 (1992).
38. Brown, N. F., and Barteau, M., *Langmuir* **8**, 862 (1992).
39. Davis, J. L., and Barteau, M., *J. Am. Chem. Soc.* **111**, 1782 (1989).
40. Houtman, C. J., and Barteau, M., *J. Catal.* **130**, 528 (1991).
41. Shekhar, R., Barteau, M., Plank, R., and Vohs, J., *J. Phys. Chem.* **101**, 7939 (1997).
42. Brown, N. F., and Barteau, M., *J. Am. Chem. Soc.* **114**, 4258 (1992).
43. Radloff, P. I., Mitchell, G. E., Greenlief, C. M., and White, J. M., *Surf. Sci.* **183**, 377 (1987).
44. Mitchell, G. E., Radloff, P. L., Greenlief, C. M., Henderson, M. A., and White, J. M., *Surf. Sci.* **183**, 403 (1987).
45. Shustorovich, *Adv. Catal.* **37**, 101 (1990).
46. McCabe, R. W., and Schmidt, L. D., *Surf. Sci.* **66**, 101 (1977).
47. Ertl, G., Neumann, M., and Streit, K. M., *Surf. Sci.* **64**, 393 (1977).
48. Aben, P. C., vanDer Eizk, H., and Oelderik, in "Proceedings, 5th International Congress on Catalysis, Palm Beach, 1972" (J. W. Hightower, Ed.), p. 717. North Holland, Amsterdam, 1973.
49. Tsuchiya, S., Amensmiya, Y., and Cvetanovic, R. J., *J. Catal.* **19**, 215 (1970).
50. Sen, B., and Vannice, M. A., *J. Catal.* **113**, 52 (1988).
51. Dandekar, A. B., Ph.D. thesis, Pennsylvania State University, 1998.
52. Shekhar, R., and Barteau, M., *Catal. Lett.* **31**, 221 (1995).
53. Davis, J. L., and Barteau, M., *Surf. Sci.* **187**, 387 (1987).
54. Carlos deJesus, J., and Zaera, F., *J. Mol. Catal. A* **138**, 237 (1999).
55. Rendulic, K. D., and Sexton, B. A., *J. Catal.* **78**, 126 (1982).
56. Davis, J. L., and Barteau, M., *Surf. Sci.* **235**, 235 (1990).
57. Singh, U. K., and Vannice, M. A., in "Proceedings, 12th International Congress on Catalysis," in press.
58. Boudart, M., *AIChE J.* **18**, 465 (1972).
59. Vannice, M. A., Hyun, S. H., Kalpakci, B., and Liauh, W. C., *J. Catal.* **56**, 358 (1979).
60. Reid, R. C., Prausnitz, J. M., and Sherwood, T. K., "The Properties of Gases and Liquids." McGraw-Hill, New York, 1977.